A High-Bandwidth and Easy-to-Integrate Parasitics-Based Switching Current Measurement Method for Fast GaN Devices

Zhiyuan Qi, *Student Member, IEEE*, Yunqing Pei, *Member, IEEE*, Laili Wang, *Senior Member, IEEE*, Zaojun Ma, *Student Member, IEEE*, Zhewei Zhang, Yan Wang, Kangping Wang, *Senior Member, IEEE*, and Xu Yang, *Senior Member, IEEE*

***Abstract*—While the very high switching speed of the gallium nitride devices can easily enable power electronics converters to operate at multi megahertz, it also brings huge challenges to switching current measurement, which is very important for the evaluation of switching performance. The conventional switching current measurement methods either have low bandwidth or have influence on layout inductance. To address these issues, this article proposes a high-bandwidth and easy-to-integrate switching current measurement method, with almost no influence on power loop layout. The proposed method utilizes the power loop trace from the source terminal of bottom switch to circuit ground as the sensing trace. By measuring the sensing voltage and considering the frequency-dependent parasitic inductance and resistance of the sensing trace, the switching current is derived based on the Fourier series theory. The simulation verification is firstly performed by using LTspice, and shows consistent results. Then, to accurately measure the sensing voltage, the used voltage probe TPP1000 is carefully modeled for measurement compensation and correction. Finally, two double pulse test (DPT) boards are designed, one with coaxial current shunt and the other without coaxial current shunt. Through DPT experiment, the accuracy of the proposed method with almost no insertion inductance is verified.**

***Index Terms*—Double pulse test (DPT), Fourier series theory, gallium nitride high electron mobility transistors (GaN HEMTs), parasitics-based switching current measurement.**

I. Introduction

THE demand for higher efficiency and power density is the driving force for the development of power electronics technologies [1], [2]. Due to having been approaching to the theoretical limit of material, the conventional silicon (Si) devices have been unable to meet the future demand for higher efficiency and power density [3], [4], [5]. The emergence of wide bandgap semiconductor devices, especially gallium nitride (GaN) devices, shows great potential to change this situation, though still at the preliminary stage of development. This is due to the superior material properties than Si material, e.g., higher electron mobility, higher saturated electron velocity, and higher electric breakdown field, enabling higher switching speed and smaller ON-state resistance to GaN devices [2], [6], [7]. By using GaN devices, the switching frequency can be easily pushed up to multi megahertz without increasing power loss, thus the higher efficiency and power density can be achieved [8], [9]. However, with the increase of switching frequency, the switching loss starts to dominate the total power loss. It is very necessary for fast GaN devices to accurately evaluate the switching loss, of which the key is to accurately measure the switching waveforms including the switching voltage and current.

To accurately capture the fast switching transient waveforms of GaN devices (only a few ns), the measurement system is required to have enough high bandwidth [10], [11], [12], [13], [14], [15]. For a typical rise/fall edge time (T_{edge}) of 2 ns, the measurement system should have a bandwidth of at least (3–5) $\times$ 175 MHz [16], [17], according to (1). Therefore, for the measurement of switching voltage, the passive voltage probes TPP1000 or TPP0850 can satisfy the requirement, as listed in Table I

$$\text{BW} = \frac{0.35}{T_{\text{edge}}}. \tag{1}$$

However, as for the measurement of switching current, it is more challenging, because it also requires small insertion impedance besides high bandwidth [10], [11], [17], [18], [19]. Among the available commercial current probes, neither

TABLE I
COMMERCIAL HIGH-BANDWIDTH PASSIVE VOLTAGE PROBES

Model	Bandwidth (MHz)	Maximum input voltage (V_{RMS})	Input capacitance (pF)	System input resistance (MΩ)
TPP1000	1000	300	3.9	10
TPP0850	850	1000	1.8	40

Manuscript received 23 February 2022; revised 17 May 2022 and 15 July 2022; accepted 17 August 2022. Date of publication 22 August 2022; date of current version 10 October 2022. This work was supported by the Key-Area Research and Development Program of Guangdong Province, China, under Grant 2020B010173001. Recommended for publication by Associate Editor K. Ngo. *(Corresponding author: Laili Wang.)*

The authors are with the State Key Laboratory of Electrical Insulation and Power Equipment, Xi'an Jiaotong University, Xi'an 710049, China. (e-mail: mambaqizhy@stu.xjtu.edu.cn; peiyq@mail.xjtu.edu.cn; llwang@mail.xjtu.edu.cn; mzj620196@stu.xjtu.edu.cn; zzw19980803@stu.xjtu.edu.cn; wy20170816@stu.xjtu.edu.cn; wangkangping@stu.xjtu.edu.cn; yangxu@mail.xjtu.edu.cn).

Color versions of one or more figures in this article are available at https://doi.org/10.1109/TPEL.2022.3200407.

Digital Object Identifier 10.1109/TPEL.2022.3200407

TABLE II
DIFFERENT TYPES OF CURRENT PROBES WITH THE HIGHEST BANDWIDTH

Type	Model	Bandwidth (MHz)	Current rating (A)
Current shunt	SDN-414-10	2000	NA
Rogowski coil	TRCP0300	30	300
Hall effect current probe	TCP0030A	120	30

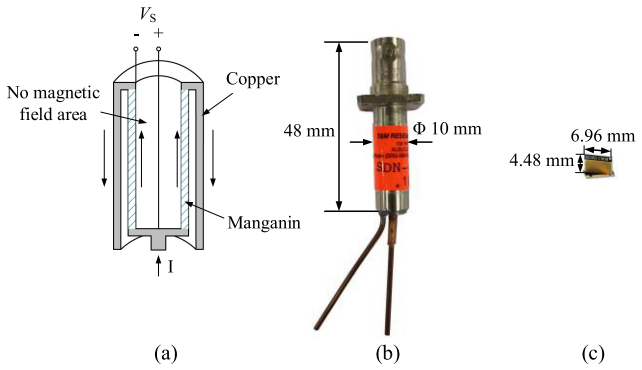

Fig. 1. (a) Cross-sectional view of coaxial current shunt. (b) Figure of coaxial current shunt SDN-414-10. (c) Figure of GaN HEMTs GS66508T.

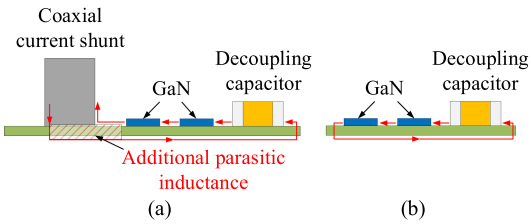

Fig. 2. Comparison of power loop area between the GaN half bridge (a) with and (b) without coaxial current shunt.

Hall-effect current probe nor Rogowski coil can be used to measure the switching current of GaN devices due to the low bandwidth. For example, the TCP0030A with the highest bandwidth among the commercial Hall effect current probes from Tektronix only has a bandwidth of 120 MHz, while the TRCP0300 with the highest bandwidth among the Rogowski coils from Tektronix only has a bandwidth of 30 MHz, as listed in Table II [20], [21]. Currently, the widely used switching current measurement method for GaN devices is the coaxial current shunt, of which the bandwidth can reach up to 2 GHz benefitting from the coaxial structure, as shown in Fig. 1(a) [19]. However, the large size relative to GaN devices will inevitably insert a significant additional inductance (can be up to several nH) into the power loop [10], [11], [14], [15], as shown in Figs. 1(b) and (c) and 2. On the one hand, the added insertion impedance can alter the switching waveforms, thus adversely affecting the measurement accuracy [12], [17], [19], [22]. On the other hand, as the high switching speed of GaN devices makes it very susceptible to the parasitic inductance, only several nH's parasitic inductance can cause serious voltage overshoot and ringing, which may break down the device [15]. Therefore, the added insertion inductance by coaxial shunt is unacceptable for the fast GaN devices.

Fig. 3. Two proposed surface mount coaxial shunt resistor PCB designs in [18].

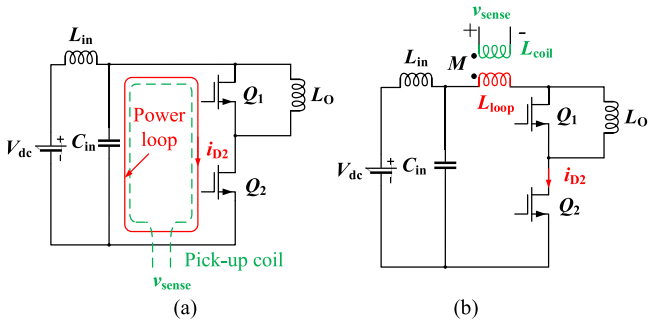

Fig. 4. Equivalent circuit schematic of the switching current measurement method by embedding a single-turn coil [19].

Great efforts have been made by researchers to reduce the inserted parasitic inductance brought by current sensors [14], [18], [19], [23], [24]. In [23], a switching current measurement method by paralleling large amounts of small footprint resistors was proposed to reduce the insertion inductance. But the accuracy is not satisfactory due to the current sharing problem caused by the skin effect and proximity effect, and the coupling effect of the power loop on measurement loop [15], [19]. Yang et al. [24] also used multiple parallel resistors to measure the switching current, and then designed an *LR* compensation network to eliminate the effect of the parasitic inductance. But the reported bandwidth is only 85 MHz, which is mainly limited by the self-resonant frequency of the compensation inductor and not enough for the GaN devices. By combing the coaxial structure and the surface mount resistors, Zhang et al. [18] proposed a surface mount coaxial shunt resistor, as shown in Fig. 3, but the inserted inductance of about 0.56 nH is still large for GaN devices. Wang et al. [19] embedded a single-turn coil in printed circuit board (PCB), as shown in Fig. 4, and utilized the coupling relationship between the pick-up coil and power loop to derive the switching current. However, the pick-up coil needs to be delicately designed, and the postprocessing and correction are very complicated. Recently, Garrido et al. [14] proposed to utilize the parasitic inductance of the power loop trace from the source terminal of bottom switch to ground to estimate the switching current. But they treated the parasitic inductance as a constant, which may affect the measurement accuracy. And only the switching current waveform within a short time period was estimated.

Different from the above methods, this article will propose an accurate high bandwidth parasitics-based switching current

measurement method for the fast GaN devices, which utilizes all the parasitic parameters of the power loop trace from the source terminal of bottom switch to the ground of circuit. The proposed method is easy to integrate and almost has no influence on power loop layout. In Section II, we will introduce and analyze the principle of the proposed switching current measurement method in detail. In Section III, the simulation verification will be given out. To ensure the accurate measurement, a probe model will be established for measurement compensation and correction in Section IV. Then, in Section V, the double pulse test (DPT) platform will be built, and the experimental comparison with the coaxial current shunt will be carried out to verify the accuracy of the proposed measurement method. A DPT board without coaxial current shunt will be also established to verify the small insertion inductance of the proposed switching current measurement method. Finally, Section VI gives out the conclusion.

II. Proposed Parasitics-Based Switching Current Measurement Method

A. Motivation and Origin

Fig. 4 shows the DPT circuit, which is widely used to assess the dynamic performance of power devices. In the DPT circuit, the upper switch Q_1 is used to provide freewheeling path for the load current $i_{\rm O}$ (current of the load inductor $L_{\rm O}$), whose gate terminal is always shorted to its source terminal. The lower switch Q_2 is the device under test (DUT), which is driven by two pulses. The first wide pulse is used to drive the load current $i_{\rm O}$ to the desired value, and during the short interval between the first wide pulse and the second narrow pulse, $i_{\rm O}$ flows through Q_1 and remains almost constant. The turn-ON and turn-OFF characteristics at the desired load current can be measured at the beginning of the second pulse and the end of the first pulse, respectively.

This section will propose a parasitics-based switching current measurement method for the fast GaN devices based on the DPT circuit. Note that the proposed method is also applicable to buck, boost, and other bridge converters. During the switching transient, the switching current of DUT Q_2 ($i_{\rm D2}$) flows through the power loop, consisting of Q_1, Q_2, and the decoupling capacitor $C_{\rm in}$. Due to the presence of the power loop parasitic parameters, a voltage will be induced across the power loop parasitic parameters mainly by the high di/dt. There is a mathematical relationship between the induced voltage and $i_{\rm D2}$, based on which we can derive $i_{\rm D2}$ from the measured induced voltage. Therefore, we can select a section of trace in power loop to detect the switching current $i_{\rm D2}$. The selected sensing trace should be the only path for $i_{\rm D2}$, and should have common ground with the circuit for convenience of measurement. In this article, the trace from the source terminal of Q_2 to the ground of the circuit was selected as the sensing trace, as shown in Fig. 5.

B. Basic Principle

To improve the measurement accuracy, all the parasitic parameters of the sensing trace are considered, including the parasitic self-inductance $L_{\rm sense}$, parasitic resistance $R_{\rm sense}$, and mutual

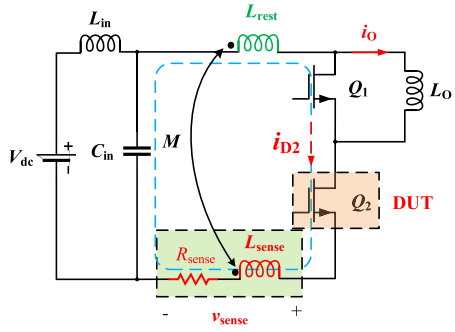

Fig. 5. Schematic of the proposed switching current measurement method based on the parasitics of a section of power loop trace.

inductance with the rest power loop trace M. Therefore, there exists the relationship between the sensing voltage $v_{\rm sense}$ and $i_{\rm D2}$, as follows:

$$v_{\rm sense} = R_{\rm sense} i_{\rm D2} + (L_{\rm sense} - M)\frac{{\rm d}i_{\rm D2}}{{\rm d}t}. \tag{2}$$

From (2), we cannot directly get the expression of $i_{\rm D2}$ about $v_{\rm sense}$, and it is also very difficult to solve this first-order non-homogeneous differential equation, as the function of $v_{\rm sense}$ about t is unknown and will be very complicated. To easily, quickly, and accurately achieve the waveform of $i_{\rm D2}$ from the measured waveforms of $v_{\rm sense}$, this article carried out a detailed derivation based on the Fourier series expansion. According to the Fourier series theory, a periodic function can be regarded as a superposition of an infinite series of sine and cosine functions with different frequencies, i.e., the Fourier series. Hence, the periodic $v_{\rm sense}$ and $i_{\rm D2}$ can be written as

$$v_{\rm sense} = V_0 + \sum_{k=1}^{\infty} V_k \sin(k\omega t + \varphi_{vk}) \tag{3}$$

$$i_{\rm D2} = I_0 + \sum_{k=1}^{\infty} I_k \sin(k\omega t + \varphi_{ik}) \tag{4}$$

where V_0 and I_0 are the dc quantities, V_k and I_k are the amplitudes at $k\omega$, φ_{vk} and φ_{ik} are the phases at $k\omega$, $\omega = 2\pi f$, and f is the fundamental frequency.

By submitting (4) into (2), it can be obtained that

$$\begin{aligned} v_{\rm sense} &= R_{\rm sense}\left[I_0 + \sum_{k=1}^{\infty} I_k \sin(k\omega t + \varphi_{ik})\right] \\ &\quad + (L_{\rm sense} - M)\sum_{k=1}^{\infty} k\omega I_k \cos(k\omega t + \varphi_{ik}) \\ &= R_{\rm sense} I_0 + \sum_{k=1}^{\infty} I_k \sqrt{{R_{\rm sense}}^2 + [k\omega(L_{\rm sense} - M)]^2} \\ &\quad \begin{bmatrix} \sin(k\omega t + \varphi_{ik})\cos\varphi_{zk} \\ +\cos(k\omega t + \varphi_{ik})\sin\varphi_{zk} \end{bmatrix} \\ &= R_{\rm sense} I_0 + \sum_{k=1}^{\infty} Z_{\rm sense} I_k \sin(k\omega t + \varphi_{ik} + \varphi_{zk}). \end{aligned} \tag{5}$$

Due to the skin effect and proximity effect, L_{sense}, R_{sense}, and M are frequency dependent, which should be considered. By using different L_{sense}, R_{sense}, and M at different frequencies, (5) can be rewritten as

$$v_{\text{sense}} = R_0 I_0 + \sum_{k=1}^{\infty} I_k \sqrt{{R_k}^2 + (k\omega L_k)^2} \begin{bmatrix} \sin(k\omega t + \varphi_{ik}) \cos\varphi_{zk} \\ + \cos(k\omega t + \varphi_{ik}) \sin\varphi_{zk} \end{bmatrix}$$

$$= R_0 I_0 + \sum_{k=1}^{\infty} Z_k I_k \sin(k\omega t + \varphi_{ik} + \varphi_{zk}) \tag{6}$$

where R_0 is the dc parasitic resistance of the sensing trace, $R_k = R_{\text{sense}}(kf)$, $L_k = L_{\text{sense}}(kf) - M(kf)$, $Z_k = \sqrt{{R_k}^2 + (k\omega L_k)^2}$, and $\varphi_{zk} = \arctan\left(\frac{k\omega L_k}{R_k}\right)$.

Then, from (3) and (6) shown at the bottom of the next page, we know that

$$v_{\text{sense}} = R_0 I_0 + \sum_{k=1}^{\infty} Z_k I_k \sin(k\omega t + \varphi_{ik} + \varphi_{zk})$$

$$= V_0 + \sum_{k=1}^{\infty} V_k \sin(k\omega t + \varphi_{vk}). \tag{7}$$

Thus, the relationship between the different frequency components of v_{sense} and i_{D2} can be obtained, based on which the switching current i_{D2} can be derived from the measured v_{sense}

$$\frac{V_0}{I_0} = R_0 \tag{8}$$

$$\frac{V_k}{I_k} = Z_k \tag{9}$$

$$\varphi_{vk} - \varphi_{ik} = \varphi_{zk}. \tag{10}$$

Note that the frequency components of the measured v_{sense} can be easily achieved by Fourier decomposition by using math software, such as MATLAB. And the frequency dependent L_{sense}, R_{sense}, and M can also be easily achieved by using finite-element analysis software Ansys Q3D Extractor. Therefore, the Fourier series of i_{D2} can be achieved by combining (3), (4), and (8)–(10), thus the waveforms of i_{D2} is achieved. The current of the top switch Q_1 (i_{D1}) can also be achieved according to $i_{\text{D1}} = i_{\text{D2}} - i_{\text{O}}$, in which i_{O} can be easily measured by using a Hall-effect current probe, e.g., TCP0030A.

III. Simulation Verification

A. Design of the Sensing Trace

To demonstrate the proposed switching current measurement method, the sensing trace was carefully designed based on a half-bridge circuit for DPT experiment, in which the GaN devices GS66508T (650 V, 30 A) from GaN Systems Inc. are used [25]. On the one hand, the sensing trace should have enough high parasitic parameters to ensure enough measurement sensitivity. On the other hand, as the fast GaN devices are very susceptible to parasitic inductance, so the sensing trace should have as small

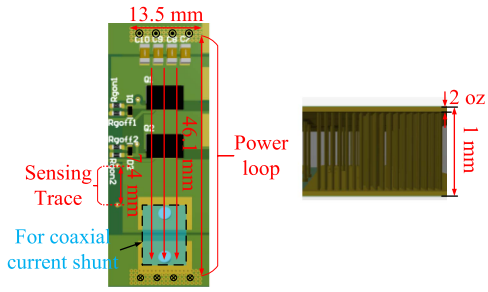

Fig. 6. Designed PCB for verifying the proposed parasitics-based switching current measurement method.

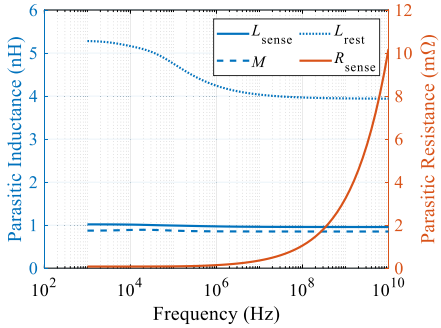

Fig. 7. Extracted parasitic parameters of sensing trace by Ansys Q3D Extractor (L_{rest} is the parasitic inductance of the rest power loop trace).

insertion impedance into power loop as possible, and cannot affect the power loop layout. In this article, the vertical loop layout is employed to reduce the power loop parasitic inductance due to the smaller power loop area than the lateral loop layout.

Then, a DPT power board with coaxial current shunt is designed, for which the sensing traces are also carefully designed. Therein, the coaxial current shunt is used for comparing with the proposed switching current measurement method. As shown in Fig. 6, the sensing trace in the PCB board with coaxial current shunt is from the source terminal of the bottom switch to the terminal of the coaxial current shunt. And the sensing trace is designed as the only path for the switching current i_{D2}. As mentioned in Section II, the sensing trace has frequency-dependent parasitic parameters, i.e., R_{sense}, L_{sense}, and M, which are very important for the accurate measurement of the switching current. Therefore, the three frequency-dependent parameters are extracted by using Ansys Q3D Extractor, in which the simulation model is based on the actual PCB layout. The simulation model was obtained by first exporting the actual PCB layout from Altium Designer to ODB++ files, and then using Ansys SIwave to convert the ODB++ files to the files readable by Ansys Q3D Extractor. The extracted parasitic parameters are shown in Fig. 7.

B. Thermal Effect on the Parasitic Resistance

Among the above three frequency-dependent parasitic parameters, i.e., L_{sense}, R_{sense}, and M, R_{sense} is also related to temperature. A temperature change on the sensing trace will

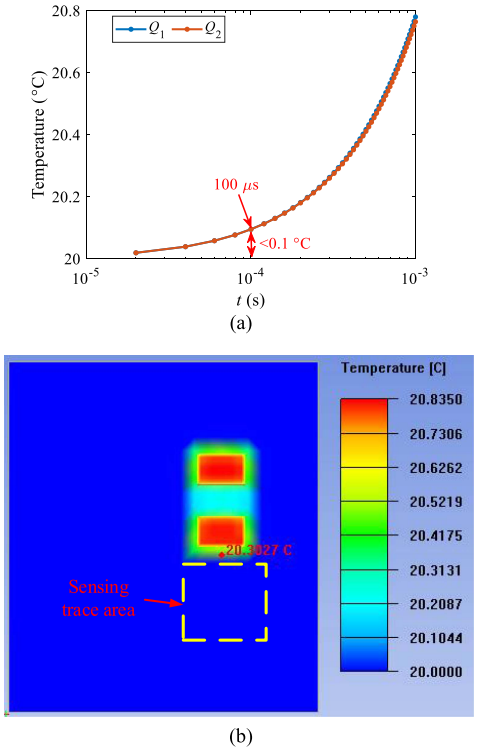

Fig. 8. Transient thermal simulation of the DPT process by using Ansys Icepak. (a) Transient temperatures of Q_1 and Q_2. (b) Thermal distribution at 1 ms.

directly increase R_{sense}, and if the temperature change is large enough and not compensated for R_{sense}, the accuracy of the proposed switching current measurement method will be affected. To study the thermal effect on R_{sense} during DPT process, a transient simulation by using Ansys Icepak was performed. For the employed GaN devices GS66508T, the current rating is 30 A and the ON-state resistance is 50 mΩ, this article will measure the switching current waveforms up to 20 A, corresponding to a maximum power loss of 20 W. Generally, the entire DPT process is within tens of microseconds. To be conservative, this article sets the power losses of both Q_1 and Q_2 to 20 W for a 1 ms transient thermal simulation. Besides, the heat transfer coefficients of both the top and bottom boundaries are set to 20 W/(K·m^2), representing natural air cooling. The transient temperatures of Q_1 and Q_2 are plotted in Fig. 8(a), and the thermal distribution at 1 ms is shown in Fig. 8(b). As we can see, the maximum temperature rise at 100 μs is only about 0.1 °C, and the maximum temperature rise at 1 ms is also lower than 1 °C (about 0.84 °C). The maximum temperature of the sensing trace occurs at the position close to Q_2, which is about 20.3027 °C. According to (9), a 1 °C temperature rise will increase the resistance of copper conductor by only 4.29‰ of the resistance at 20 °C [26]. Therefore, the temperature effect on the parasitic resistance of the sensing trace during DPT process can be ignored. If the proposed method is applied to the converter applications, the temperature effect on the parasitic resistance should be considered and compensated as

$$R = R_{\text{ref}}\,[1+\alpha(T-T_{\text{ref}})] \tag{11}$$

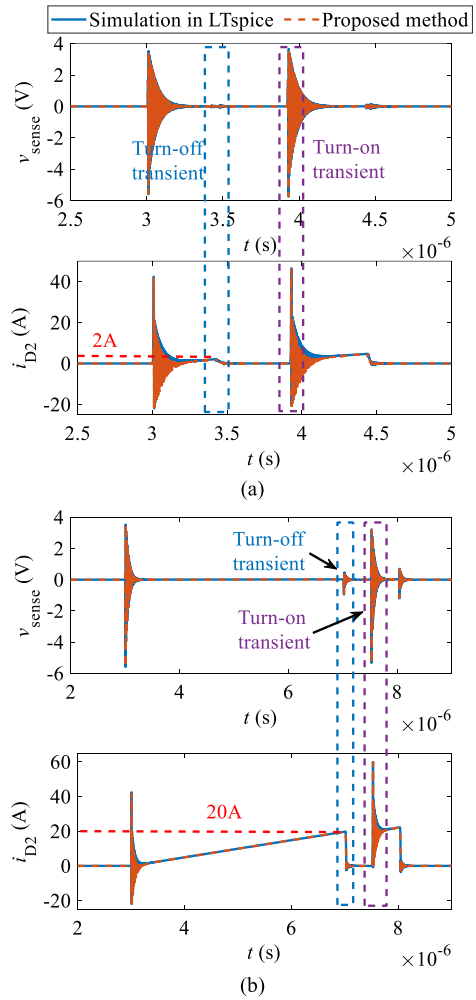

Fig. 9. Switching current comparison at the output current of (a) 2 A and (b) 20 A between the proposed parasitics-based method and the simulation in LTspice.

where R is the conductor resistance at temperature T, R_{ref} is the conductor resistance at reference temperature T_{ref} (20 °C in this article), and α is the temperature coefficient of resistance for copper material, 4.29×10^{-3} °C^{-1}.

C. Simulation Comparison

In order to preliminarily verify the effectiveness of the proposed switching current measurement method, the DPT simulation was carried out by using LTspice. As the frequency dependency of the parasitic parameters cannot be simulated in LTspice, so this article uses the values at the frequency of 100 MHz (comparable to the high-frequency oscillations of the switching waveforms) for simulation comparison. As mentioned in Section II, it is first required to measure the voltage across the sensing trace v_{sense}, then based on the method in Section II, the switching current of DUT i_{D2} can be derived by using MATLAB. The switching current waveforms at the current of 2 and 20 A are compared in Fig. 9(a) and (b), and the enlarged switching current waveforms during turn-ON and turn-OFF process are plotted in Fig. 10(a) and (b). It can be seen that, at the load current of no matter 2 or 20 A, the obtained

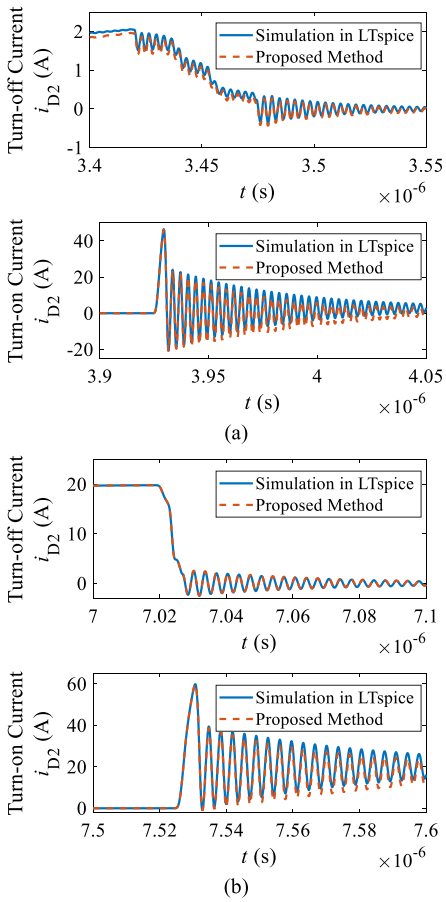

Fig. 10. Enlarged switching current comparison at the output current of (a) 2 A and (b) 20 A between the proposed parasitics-based method and the simulation in LTspice.

switching current waveforms by the proposed parasitics-based measurement method have good consistency with the switching current waveforms by simulation in LTspice. Therefore, it can be preliminarily verified that the proposed switching current measurement method can accurately measure both small and large switching current.

IV. Measurement Compensation and Correction

As mentioned in Section II, the key to accurately measure the switching current by using the proposed method is the accurate measurement of v_{sense}. Although the 1 GHz high-bandwidth passive voltage probe TPP1000 is used for experimental measurement, it is not enough to ensure the measurement accuracy. Special attentions should be paid to the effects of the voltage probe on the measurement accuracy, including the load effect and the effect of probe bandwidth.

A. Modeling of Voltage Probe

To understand the effects of voltage probe, it is very essential to accurately model the voltage probe. As Azpurua et al. [27] have made great deal of work on the probe modeling, so this article will make a modification to the probe model to improve the accuracy. Fig. 11 shows the equivalent circuit model of the probe-oscilloscope system connected to the test point. As we can see, the passive voltage probe consists of four parts, i.e., probe tip, coaxial cable, compensation box, and ground wire. The probe tip is modeled by the parallel circuit of the probe series resistance R_{P}, and the probe input capacitance C_{P} in series with the resistance R_{P1}, in which R_{P} and C_{P} are 9 MΩ and 3.9 pF, respectively [28]. The coaxial cable, which is lossy transmission line, can be modeled by a sequence of line elements (R, L, G, C) [29], [30]. The compensation box is modeled by R_{trim}, R_{comp}, and C_{comp}. R_{S} and C_{S} are the input resistance and capacitance of the oscilloscope (MSO64 6-BW-1000A), and R_{S1} is a series resistance with C_{S}, in which R_{S} and C_{S} are 1 MΩ and 14.5 pF, respectively [31]. The ground inductance L_{P} is related to the grounding technology, which are about 10 and 150 nH, respectively, for the 1/2″ ground spring and 6″ ground wire [32].

TABLE III
Obtained Model Parameters of TPP1000

Parameters	Value	Parameters	Value
R	2.5 Ω	R_{P1}	135 Ω
L	2.5 nH	R_{trim}	225 Ω
G	0.1 nS	R_{comp}	72 Ω
C	0.058 pF	C_{comp}	19.44 pF
n	20	R_{S1}	50 Ω

In the model, the parameters R_{P1}, R, L, G, C, R_{trim}, R_{comp}, C_{comp}, and R_{S1} are still unknown, and cannot be obtained from the datasheet of probes. To achieve them, a parametric sweep ac analysis was performed by using Saber software to make the impedance characteristics of the proposed model well match with that of TPP1000 [27], [28]. During the parametric sweep simulation, the relationship should be satisfied as follows:

$$\frac{R_{\text{P}}}{R_{\text{S}}} = \frac{C_{\text{cable}} + C_{\text{comp}} + C_{\text{S}}}{C_{\text{P}}} \tag{12}$$

where C_{cable} equals to C times the number of (R, L, G, C) cells n. Through careful parametric sweep simulation, the impedance characteristics of the proposed probe-oscilloscope system model well matches with that of TPP1000, as shown in Fig. 12(a), and the obtained parameters are listed in Table III.

B. Load Effect of Voltage Probe

When the voltage probe is connected to the circuit to measure the voltage of the sensing trace, it will act as a load to draw current from the circuit, which will affect the operation of circuit and further the measurement results. To minimize the load effect, the impedance of probe-oscilloscope system $|Z_{\text{P}}(s)|$ should be much higher than that of the sensing trace $|Z_{\text{sense}}(s)|$, in which

$$Z_{\text{sense}}(s) = s(L_{\text{sense}} - M) + R_{\text{sense}}. \tag{13}$$

In Fig. 12(b), $|Z_{\text{sense}}(s)|$ is compared with $|Z_{\text{P}}(s)|$ at $L_{\text{P}} =$ 10 and 150 nH. It can be seen that $|Z_{\text{P}}(s)|$ remains over 100 times higher than $|Z_{\text{sense}}(s)|$ within the frequency range from

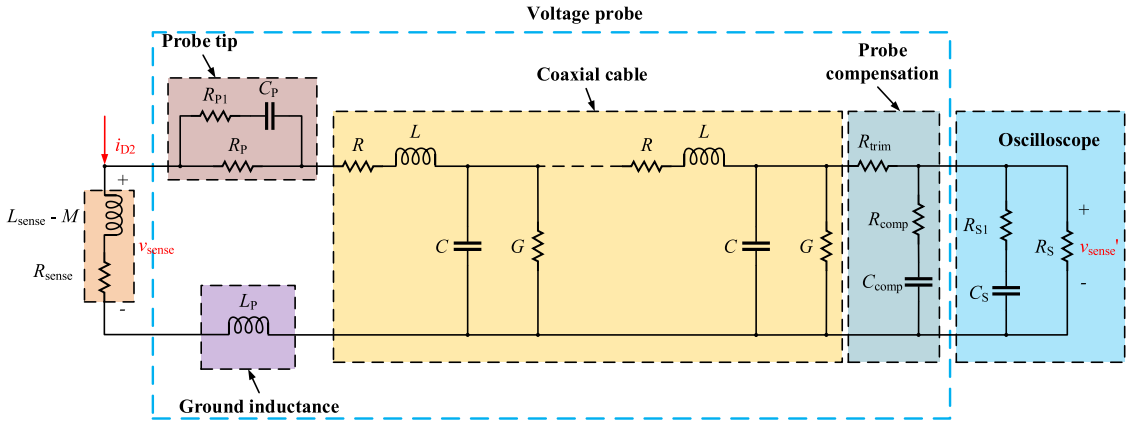

Fig. 11. Equivalent circuit model of the probe-oscilloscope system connecting to circuit.

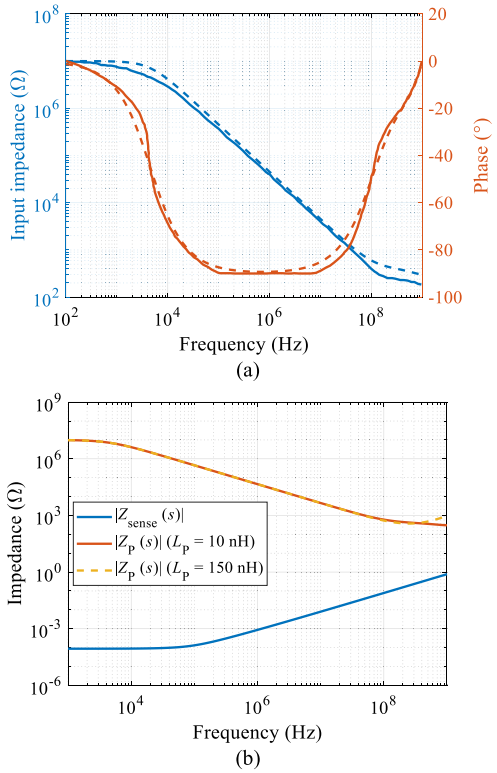

Fig. 12. (a) Impedance characteristics of TPP1000 (solid line: curve fitting from datasheet, dash line: proposed model). (b) Impedance comparison between the probe-oscilloscope system and sensing trace.

1 kHz to 1 GHz. Therefore, due to the very small parasitic capacitance of TPP1000, the load effect of passive voltage probe on measurement can be ignored regardless of ground inductance.

C. Effect of Bandwidth on Measurement

Besides the requirement of weak loading effect, the probe circuit from probe tip to oscilloscope input should also have as small attenuation and phase shift as possible to ensure enough high signal fidelity, which depends on the bandwidth of probe [16]. Based on the obtained probe model of TPP1000 in Saber

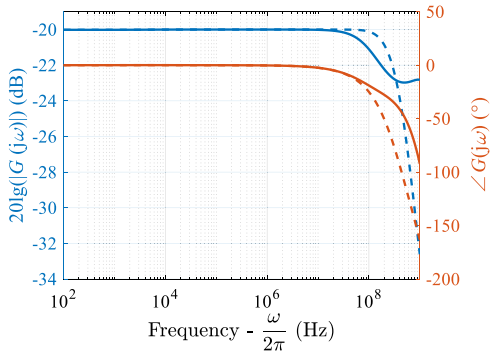

Fig. 13. Transfer characteristics of TPP1000 from test point to oscilloscope input (solid line: $L_P = 10$ nH, dash line: $L_P = 150$ nH).

software, the transfer characteristics of TPP1000 from test point to oscilloscope input can also be achieved. As shown in Fig. 13, the gain from probe tip to oscilloscope input keeps flat until about 20 MHz, after which it starts to gradually drop to 3 dB at 1 GHz. Meanwhile, when the frequency is higher than about 10 MHz, a phase difference starts to appear between the signal at probe tip and the signal at oscilloscope input. For the high-frequency GaN devices, the frequency of oscillation during switching transient usually can be higher than 100 MHz, so the measured waveforms will be distorted. Importantly, the ground inductance has effect on the bandwidth of probe. The 1-GHz bandwidth of TPP1000 is measured when the 1/2″ spring ground is used. If the 6″ ground wire is used which has about 150 nH parasitic inductance, the bandwidth will be further reduced, as shown in Fig. 13. To achieve a faithful measurement of the sensing voltage v_{sense}, which is very important for the accurate derivation of the switching current i_{D2}, it is recommended to use the ground spring as the ground method. More importantly, the measured sensing voltage v_{sense}' still should be compensated and corrected.

D. Measurement Compensation and Correction

As mentioned above, due to the bandwidth limit, there are some differences in the amplitudes and phases of v_{sense}' and

v_{sense}, so it is very necessary to correct and compensate the measured $v_{\text{sense}}{}'$ to achieve the actual v_{sense}. Both $v_{\text{sense}}{}'$ and v_{sense} can be regarded as the superposition of an infinite series of sine and cosine functions with different frequencies, as shown in (3) and in the following equation:

$$v_{\text{sense}}{}' = V_0{}' + \sum_{k=1}^{\infty} V_k{}' \sin\left(k\omega t + \varphi_{vk}{}'\right). \tag{14}$$

Assuming the probe-oscilloscope system is linear time-invariant, there is

$$\frac{v_{\text{sense}}{}'(\text{j}\omega)}{v_{\text{sense}}(\text{j}\omega)} = G(\text{j}\omega) = |G(\text{j}\omega)|\angle G(\text{j}\omega) \tag{15}$$

where $G(\text{j}\omega)$ is the complex value transfer function of the probe, ω is the angular frequency, and $G(\text{j}\omega)$ can be easily obtained from Fig. 13, according to (15). From (3), (14), and (15), we can get

$$V_0 = \frac{V_0{}'}{|G(\text{j}0)|} \tag{16}$$

$$V_k = \frac{V_k{}'}{|G(\text{j}k\omega)|} \tag{17}$$

$$\varphi_{vk} = \varphi_{vk}{}' - \angle G(\text{j}k\omega). \tag{18}$$

Therefore, the measured $v_{\text{sense}}{}'$ can be compensated to achieve the actual v_{sense}, based on which the switching current i_{D2} can be accurately derived.

V. Experimental Verification

A. Establishment of the DPT Platform

To verify the accuracy of the proposed switching current measurement method, a DPT board was designed in which a 2-GHz bandwidth coaxial current shunt SDN-414-10 was installed as a comparison benchmark for the proposed switching current measurement method, as shown in Fig. 14(a). To extend the measurement frequency range as much as possible, this article reduces the gate resistance as much as possible to increase the dv/dt and di/dt. However, the gate resistance cannot be infinitely reduced; otherwise, an enough high gate-source overshoot voltage will be caused to break down the gate-source electrode of GaN devices. To ensure the gate-source overshoot voltage smaller than 0.5 V with sufficient safety margin, the damping coefficient of the driving loop ζ as shown in (19) should be greater than 0.62, according to (20) [33], [34]

$$R_{\text{Gon}} = 2\zeta\sqrt{\frac{L_{\text{Gon}}}{C_{\text{ISS}}}} \tag{19}$$

$$\text{OvershootVoltage} = V_{\text{g}} \cdot \text{e}^{-\frac{\zeta\cdot\pi}{\sqrt{1-\zeta^2}}} \tag{20}$$

where L_{GON} is the parasitic inductance of turn-ON loop (about 7.63 nH by simulation in Ansys Q3D Extractor), C_{ISS} is the input capacitance of GS66508T (242 pF), and V_{g} is the driving voltage (6 V is recommended). Therefore, the turn-ON gate resistance should be larger than 6.96 Ω. As the isolated half-bridge driver Si8273GBD-IS1 is employed in this article, its internal turn-ON resistance is 2.7 Ω, and the internal gate resistance of GS66508T is 1.1 Ω. Therefore, the calculated minimum external gate resistance is 3.16 Ω. In this article, the external turn-ON gate resistance was selected as 3.3 Ω, and the external turn-OFF resistance was selected as 0 Ω.

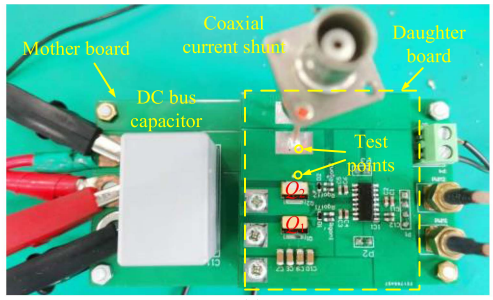

(a)

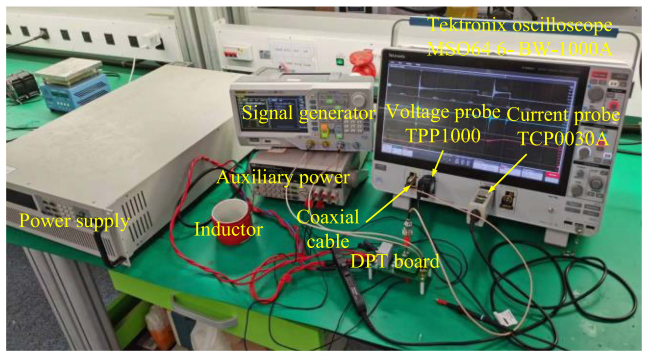

(b)

Fig. 14. (a) Prototype of DPT board with coaxial current shunt. (b) DPT experimental platform.

Then, the DPT experimental platform was established, in which an air core inductor of about 50 μH is used as the output inductor to prevent saturation under high current, as shown in Fig. 14(b). The signal generator DG4062 is used to generate the double pulse signal for gate driver, the auxiliary power is used to power the gate driver, and the power supply is used to provide the dc bus voltage. The 1-GHz high-bandwidth oscilloscope MSO64 6-BW-1000A was used, equipped with the 1-GHz passive voltage probe TPP1000 to measure the sensing voltage v_{sense}, the coaxial cable with BNC connector to measure the switching current i_{D2} by coaxial current shunt, and the current probe TCP0030A to measure the current waveform of output inductor i_{O}. Note that, in the DPT board with coaxial current shunt, the current shunt is connected in reverse series in the power loop, in which the current shunt BNC output case is connected to the source terminal of Q_2 [35].

B. Switching Current Waveforms Comparison

By performing the DPT experiment, the waveforms of v_{sense}, i_{D2}, and I_{L} were measured at the output current of about 2, 5, 10, and 20 A, as shown in Fig. 15(a)–(d). Then, the waveforms were exported from the oscilloscope for postprocessing. According to the implementation process of the proposed switching current measurement method given in Fig. 16, a smooth denoise process

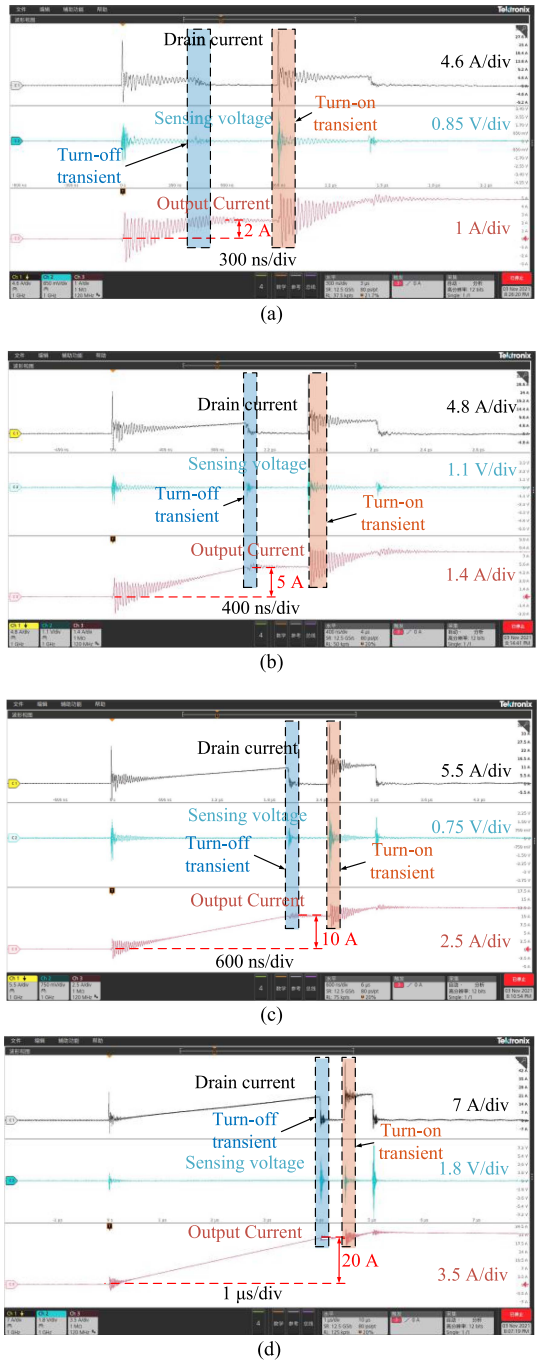

Fig. 15. Experimental waveforms at the output current of about (a) 2 A, (b) 5 A, (c) 10 A, and (d) 20 A.

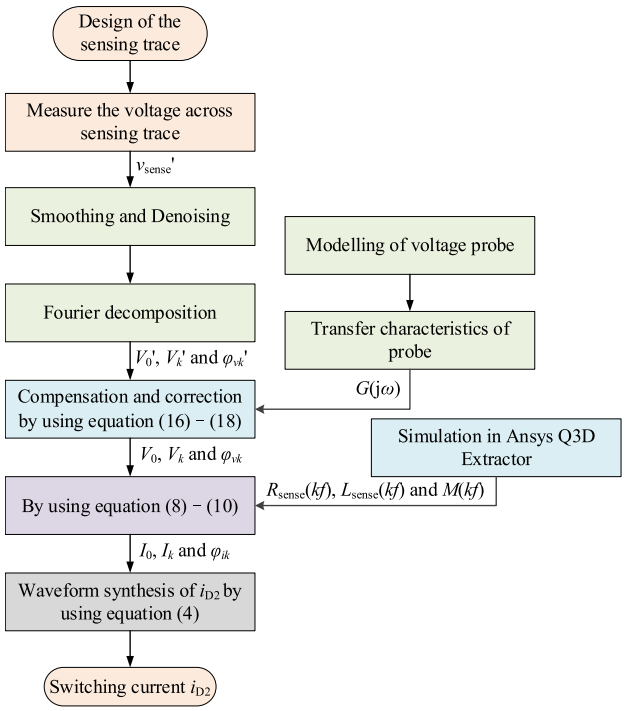

Fig. 16. Flowchart of the proposed parasitics-based switching current measurement method.

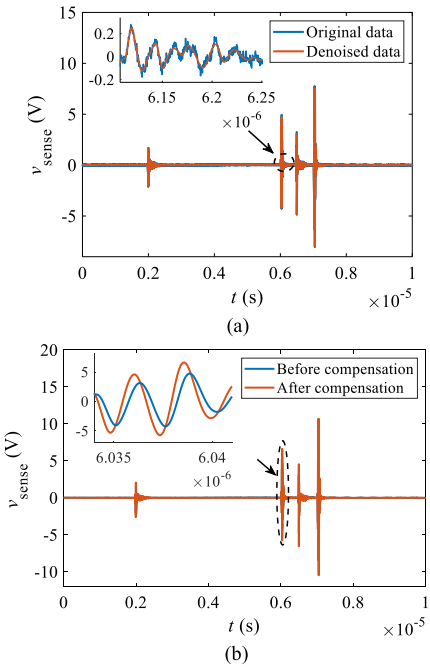

Fig. 17. (a) Denoise of the measured sensing voltage. (b) Compensation based on the probe-oscilloscope system model.

is first required for the measured sensing voltage v_{sense}', because the measured waveforms by oscilloscope always contain noises, which are Gaussian white noise [36]. In this article, the wavelet signal denoiser toolbox in MATLAB was used to denoise the waveform of v_{sense}', as shown in Fig. 17(a). Then, after the Fourier decomposition of v_{sense}' by using MATLAB, the compensation and correction was performed on v_{sense}' based on the established probe model. The waveforms before and after compensation are compared in Fig. 17(b). It can be clearly seen that after compensation, the amplitude of the waveform is magnified and the phase is moved forward. As mentioned in Section III, the frequency-dependent parasitic parameters of the sensing trace were extracted by using Ansys Q3D Extractor based on the actual PCB layout, as shown in Fig. 7. According to (3), (4), and (7)–(9), the proposed method was implemented in MATLAB, and thus the switching current i_{D2} was obtained.

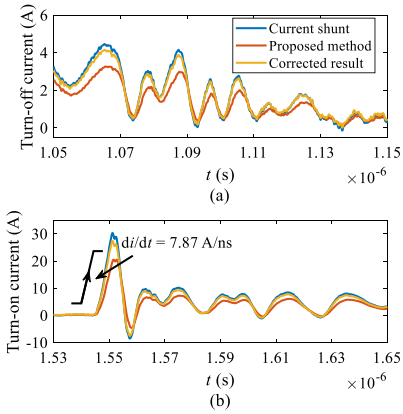

Fig. 18. Switching current waveforms comparison at the output current of about 2 A. (a) Turn-OFF current waveforms. (b) Turn-ON current waveforms.

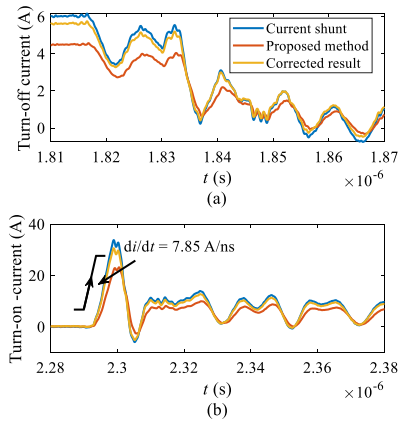

Fig. 19. Switching current waveform comparison at the output current of about 5 A. (a) Turn-OFF current waveforms. (b) Turn-ON current waveforms.

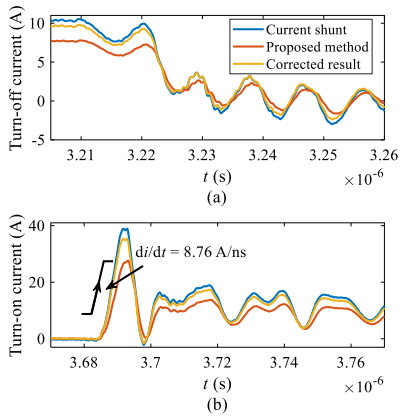

Fig. 20. Switching current waveform comparison at the output current of about 10 A. (a) Turn-OFF current waveforms. (b) Turn-ON current waveforms.

In Figs. 18 –21, the turn-ON and turn-OFF current waveforms at the output current of about 2, 5, 10, and 20 A are compared with those measured by coaxial current shunt, respectively. As we can see, due to the use of the very small turn-ON gate resistance, the maximum di/dt during turn-ON process at the output current of 2, 5, 10, and 20 A can be as high as about 7.87, 7.85, 8.76, and 9.5 A/ns, respectively. When measuring such high-speed

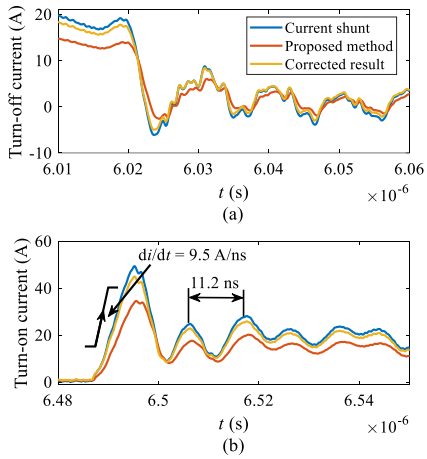

Fig. 21. Switching current waveform comparison at the output current of about 20 A. (a) Turn-OFF current waveforms. (b) Turn-ON current waveforms.

switching current, due to the effect of the probe, the switching current waveforms directly derived from the measured v_{sense} has a relatively larger error, in which the amplitude is smaller than that of coaxial current shunt, and the phase lags behind that of the coaxial current shunt. Benefitting from the compensation by considering the probe model, the amplitude is amplified and the phase is moved forward. In theory, the effect of probe on measurement can be minimized, and the measurement will not be limited by the probe bandwidth, but only related to the maximum frequency by Fourier decomposition in MATLAB. As the sampling rate of the oscilloscope decides the maximum frequency by Fourier decomposition, the 25 GS/s high sampling rate of the used oscilloscope MSO64 6-BW-1000A can help to achieve high measurement accuracy. It can be seen from Figs. 18–21, the corrected switching current waveforms by the proposed method match better with those by coaxial current shunt, but there is still an error. Through analysis, there are mainly two reasons. The first is the PCB fabrication error, which makes the PCB structure parameters (including copper thickness and board thickness) used in simulation slightly different from the actual parameters, thus resulting in simulation error of the parasitic parameters of the sensing trace. The simulation error will directly affect the accuracy of the proposed method. The second reason is that the established probe model may have error, which will affect the compensation effect. To improve the accuracy of the proposed method, in our future article, more in-depth research on the probe modeling will be conducted to uncover the effect on measurement. Nevertheless, the accuracy of the proposed switching current measurement method including probe-model-based compensation can be verified.

C. *Verification of the Small Insertion Inductance*

To verify that the proposed switching current measurement method almost has no insertion inductance to power loop, a DPT board without coaxial current shunt was designed, as shown in Fig. 22(a). The frequency-dependent parasitic parameters were also extracted by using Ansys Q3D Extractor, as shown in Fig. 22(b). By conducting the DPT experiment, the waveforms

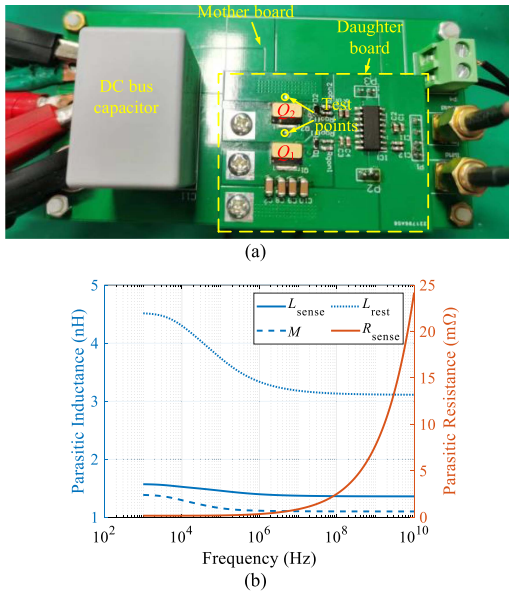

Fig. 22. DPT board without coaxial current shunt. (a) Experimental prototype. (b) Extracted parasitic parameters of the sensing trace.

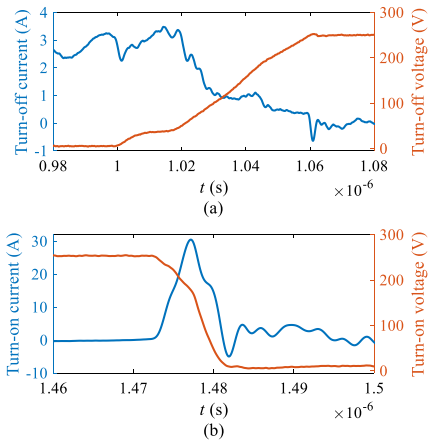

Fig. 23. Switching waveforms at the output current of about 2 A. (a) Turn-OFF current waveforms. (b) Turn-ON current waveforms.

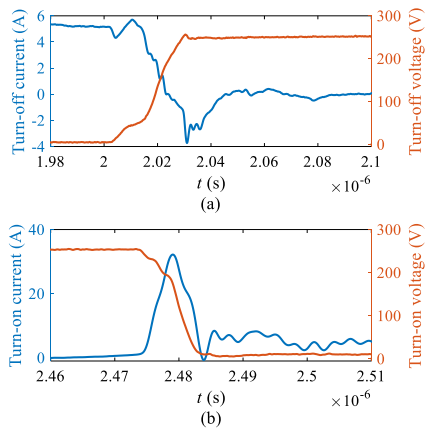

Fig. 24. Switching waveforms at the output current of about 5 A. (a) Turn-OFF current waveforms. (b) Turn-ON current waveforms.

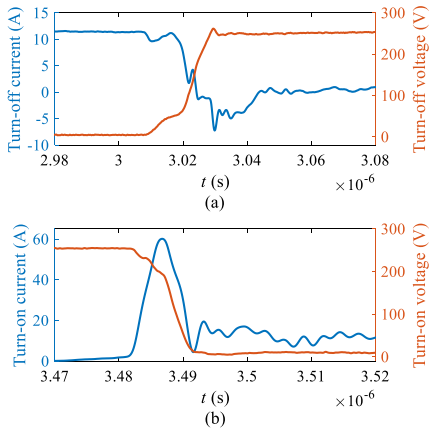

Fig. 25. Switching waveforms at the output current of about 10 A. (a) Turn-OFF current waveforms. (b) Turn-ON current waveforms.

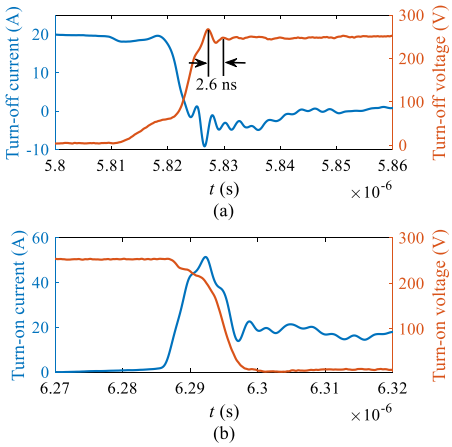

Fig. 26. Switching waveforms at the output current of about 20 A. (a) Turn-OFF current waveforms. (b) Turn-ON current waveforms.

of $v_{\rm sense}$ and the switching voltage $v_{\rm DS2}$ were also measured at the output current of about 2, 5, 10, and 20 A, respectively. By implementing the proposed method in MATLAB, the switching currents $i_{\rm D2}$ were derived. The switching current and voltage waveforms at the output current of about 2, 5, 10, and 20 A are plotted in Figs. 23–26, respectively. As we can see, the proposed method can accurately measure the switching current waveforms and have a consistent pace with the switching voltage. Moreover, the oscillation period during switching transient is only about 2.6 ns, as shown in Fig. 26, while the oscillation period of the DPT board with coaxial current shunt is about 11.2 ns (as shown in Fig. 21). According to (21), the power loop inductances of the DPT board with and without coaxial current shunt are about 1.95 and 36.3 nH, respectively. Note that, the large power loop inductance of the DPT board with coaxial shunt is caused by the long legs of the coaxial current shunt and the additional power loop area. The power loop inductance of the DPT board without coaxial current shunt can be further reduced by optimizing power loop layout, without affecting the switching current measurement by the proposed method. Therefore, the effectiveness of the proposed parasitics-based switching current measurement

method regarding the no insertion inductance is verified

$$L_{\text{loop}} = \frac{T^2}{4\pi^2 C_{\text{OSS}}} \tag{21}$$

where C_{OSS} is the output capacitance of the employed GaN devices GS66508T at 250 V (about 87.6 pF) [25].

VI. Conclusion

The fast GaN devices poses huge challenges to the switching current measurement, and the conventional switching current measurement method either having low bandwidth or having influence on the layout inductance cannot meet the measurement requirement of GaN devices. To address these issues, this article proposed a high-bandwidth and easy-to-integrate switching current measurement method, with almost no influence on power loop layout. The proposed method utilizes the power loop trace from the source terminal of bottom switch to circuit ground as the sensing trace. Based on the Fourier series theory, the relationship between the parasitic inductance and resistance of the sensing trace, each frequency components of the sensing voltage and the switching current was derived. Based on the actual PCB layout, the parasitic inductance and resistance of the sensing trace can be extracted by using Ansys Q3D Extractor. Thus, the switching current can be derived from the measured sensing voltage. Careful simulation verification was first conducted by using LTspice, and shows consistent results. Then, to accurately measure the sensing voltage for experimental verification, which is very important for the accurate derivation of the switching current, the used probe TPP1000 was modeled for measurement compensation and correction. Finally, two DPT boards were designed based on the 650 V/30 A GaN device GS66508T, one with coaxial current shunt and the other without coaxial current shunt. Through the DPT experiment, the accuracy of the proposed switching current measurement method with almost no insertion inductance was verified.

References

[1] X. Huang, "High frequency GaN characterization and design considerations," Ph.D. dissertation, Virginia Polytech. Inst. State Univ., Blacksburg, VA, USA, 2016.

[2] Z. Qi et al., "An accurate datasheet-based full-characteristics analytical model of GaN HEMTs for deadtime optimization," *IEEE Trans. Power Electron.*, vol. 36, no. 7, pp. 7942–7955, Jul. 2021.

[3] J. Chen, X. Du, Q. M. Luo, X. Y. Zhang, P. J. Sun, and L. Zhou, "A review of switching oscillations of wide bandgap semiconductor devices," *IEEE Trans. Power Electron.*, vol. 35, no. 12, pp. 13182–13199, Dec. 2020.

[4] R. L. Xie, H. X. Wang, G. F. Tang, X. Yang, and K. J. Chen, "An analytical model for false turn-on evaluation of high-voltage enhancement-mode GaN transistor in bridge-leg configuration," *IEEE Trans. Power Electron.*, vol. 32, no. 8, pp. 6416–6433, Aug. 2017.

[5] C. Chen, "A review of SiC power module packaging: Layout, material system and integration," *CPSS Trans. Power Electron. Appl.*, vol. 2, no. 3, pp. 170–186, 2017.

[6] E. A. Jones, F. Wang, and D. Costinett, "Review of commercial GaN power devices and GaN-based converter design challenges," *IEEE J. Emerg. Sel. Topics Power Electron.*, vol. 4, no. 3, pp. 707–719, Sep. 2016.

[7] J. Millan, P. Godignon, X. Perpina, A. Perez-Tomas, and J. Rebollo, "A survey of wide bandgap power semiconductor devices," *IEEE Trans. Power Electron.*, vol. 29, no. 5, pp. 2155–2163, May 2014.

[8] K. P. Wang, X. Yang, H. C. Li, H. Ma, X. J. Zeng, and W. J. Chen, "An analytical switching process model of low-voltage eGaN HEMTs for loss calcul4ation," *IEEE Trans. Power Electron.*, vol. 31, no. 1, pp. 635–647, Jan. 2016.

[9] L. L. Wang, Y. Q. Pei, X. Yang, X. Z. Cui, and Z. A. Wang, "Three-dimensional integration of high frequency DC/DC converters based on LTCC technology," in *Proc. IEEE 6th Int. Power Electron. Motion Control Conf.*, 2009, pp. 537–540.

[10] K. Li, A. Videt, and N. Idir, "Using current surface probe to measure the current of the fast power semiconductors," *IEEE Trans. Power Electron.*, vol. 30, no. 6, pp. 2911–2917, Jun. 2015.

[11] S. Sandler, "Faster-switching GaN: Presenting a number of interesting measurement challenges," *IEEE Power Electron. Mag.*, vol. 2, no. 2, pp. 24–31, Jun. 2015.

[12] F. Wang, Z. Zhang, and E. A. Jones, *Characterization of Wide Bandgap Power Semiconductor Devices*. London, U.K.: Institution Eng. Technol., 2018.

[13] U. J. Kim, M. S. Song, and R. Y. Kim, "PCB-based current sensor design for sensing switch current of a nonmodular GaN power semiconductor," *Energies*, vol. 13, no. 19, Oct. 2020, Art. no. 5161.

[14] D. Garrido, I. Baraia-Etxaburu, J. Arza, and M. Barrenetxea, "Simple and affordable method for fast transient measurements of SiC devices," *IEEE Trans. Power Electron.*, vol. 35, no. 3, pp. 2933–2942, Mar. 2020.

[15] J. Lautner and B. Piepenbreier, "Impact of current measurement on switching characterization of GaN transistors," in *Proc. IEEE Workshop Wide Bandgap Power Devices Appl.*, 2014, pp. 98–102.

[16] Tektronix Inc., "ABCs of probes 60W-6053-15," 2018. [Online]. Available: https://download.tek.com/document/ABCs%20of%20Probes%2060W-6053-15.pdf

[17] Z. Y. Zhang, B. Guo, F. Wang, E. A. Jones, L. M. Tolbert, and B. J. Blalock, "Methodology for wide band-gap device dynamic characterization," *IEEE Trans. Power Electron.*, vol. 32, no. 12, pp. 9307–9318, Dec. 2017.

[18] W. Zhang, Z. Y. Zhang, F. Wang, E. V. Brush, and N. Forcier, "High-bandwidth low-inductance current shunt for wide-bandgap devices dynamic characterization," *IEEE Trans. Power Electron.*, vol. 36, no. 4, pp. 4522–4531, Apr. 2021.

[19] K. P. Wang, X. Yang, H. C. Li, L. L. Wang, and P. Jain, "A high-bandwidth integrated current measurement for detecting switching current of fast GaN devices," *IEEE Trans. Power Electron.*, vol. 33, no. 7, pp. 6199–6210, Jul. 2018.

[20] Tektronix Inc., TCP0030A current probe, 2017. [Online]. Available: https://www.tek.com.cn/manual/current-probe/tcp0030a-current-probe

[21] Tektronix Inc., TRCP0300 Rogowski current probes, 2019. [Online]. Available: https://www.tek.com.cn/datasheet/current-probes-0

[22] M. d. R. Alex Lidow, J. Strydom, D. Reusch, and J. Glaser, *GaN Transistors for Efficient Power Conversion III*. Hoboken, NJ, USA: Wiley, 2020, p. 384.

[23] M. Danilovic, Z. Chen, R. X. Wang, F. Luo, D. Boroyevich, and P. Mattavelli, "Evaluation of the switching characteristics of a gallium-nitride transistor," in *Proc. IEEE Energy Convers. Congr. Expo.*, 2011, pp. 2681–2688.

[24] C. Z. Yang et al., "Analysis and design of a low1-cost well-performance and easy-to-design current sensing circuit suitable for SiC MOSFETS," *IEEE Trans. Power Electron.*, vol. 35, no. 12, pp. 13356–13366, Dec. 2020.

[25] GaN Systems Inc., "GS66508T Top-side cooled 650 V E-mode GaN transistor datasheet," 2020. [Online]. Available: https://gansystems.com/wp-content/uploads/2020/04/GS66508T-DS-Rev-200402.pdf

[26] E. ToolBox, "Resistivity and conductivity—temperature coefficients common materials," 2003. [Online]. Available: https://www.engineeringtoolbox.com/resistivity-conductivity-d_418.html

[27] M. A. Azpurua, M. Pous, and F. Silva, "Time and frequency domain characterization of switching losses in GaN FETs power converters," *IEEE Trans. Power Electron.*, vol. 37, no. 3, pp. 3219–3232, Mar. 2022.

[28] Tektronix Inc., TPP1000 voltage probe, 2018. [Online]. Available: https://www.tek.com/en/passive-probe-manual/tpp1000-0

[29] K. Ammous, H. Morel, and A. Ammous, "Inverse models of voltage and current probes," *IEEE Trans. Instrum. Meas.*, vol. 60, no. 12, pp. 3898–3906, Dec. 2011.

[30] K. Ammous, H. Morel, and A. Ammous, "Analysis of power switching losses accounting probe modeling," *IEEE Trans. Instrum. Meas.*, vol. 59, no. 12, pp. 3218–3226, Dec. 2010.

[31] Tektronix Inc., MSO64 6-BW-1000A oscilloscope, 2019. [Online]. Available: https://www.tek.com.cn/datasheet/6-series-mso

[32] S. Biswas, D. Reusch, M. De Rooij, and T. Neville, "Evaluation of measurement techniques for high-speed GaN transistors," in *Proc. 5th Workshop Wide Bandgap Power Devices Appl.*, 2017, pp. 105–110.
[33] Z. Qi, Y. Pei, L. Wang, Q. Yang, and K. Wang, "A highly integrated PCB embedded GaN full-bridge module with ultralow parasitic inductance," *IEEE Trans. Power Electron.*, vol. 37, no. 4, pp. 4161–4173, Apr. 2022.
[34] D. Reusch, D. Gilham, Y. P. Su, and F. C. Lee, "Gallium nitride based 3D integrated non-isolated point of load module," in *Proc. 27th Annu. IEEE Appl. Power Electron. Conf. Expo.*, 2012, pp. 38–45.
[35] GaN Systems Inc., "650V GaN E-HEMT evaluation board technical manual," 2020. [Online]. Available: https://gansystems.com/wp-content/uploads/2021/06/GS665xxT-EVBDB2_Technical-Manual_Rev_200525.pdf
[36] M. H. Dong, H. Li, S. Yin, Y. Z. Wu, and K. Y. See, "A postprocessing-technique-based switching loss estimation method for GaN devices," *IEEE Trans. Power Electron.*, vol. 36, no. 7, pp. 8253–8266, Jul. 2021.

Zhiyuan Qi (Student Member, IEEE) was born in Henan Province, China, in 1989. He received the B.S. and M.S. degrees in electrical engineering and automation from the Harbin Engineering University, Harbin, China, in 2012 and 2015, respectively. He is currently working toward the Ph.D. degree in electrical engineering with the Xi'an Jiaotong University, Xi'an, China.

His research interests include the packaging and integration of wide bandgap power semiconductors and high-frequency power conversion technologies.

Yunqing Pei (Member, IEEE) was born in 1969. He received the B.S. and M.S. degrees in electrical engineering, and the Ph.D. degree in power electronics from the Xi'an Jiaotong University, Xi'an, China, in 1991, 1994, and 1999, respectively.

He became a Faculty Member of the Xi'an Jiaotong University, where he is currently a Professor with the Xi'an Jiaotong University. From February 2006 to February 2007, he was a Visiting Scholar with the Center of Power Electronics Systems, Virginia Polytechnic Institute and State University, Blacksburg, VA, USA. His research interests include the high-power inverters, switch mode power supply, and converters in distributed generation systems.

Laili Wang (Senior Member, IEEE) received the B.S., M.S., and Ph.D. degrees from the School of Electrical Engineering, Xi'an Jiaotong University, Xi'an, China, in 2004, 2007, and 2011, respectively.

Since 2011, he has been a Postdoctoral Research Fellow with the Department of Electrical Engineering, Queen's University, Kingston, ON, Canada.

From 2014 to 2017, he was an Electrical Engineer with the Sumida, Kingston, ON, Canada. In 2017, he became a Full Professor with the Xi'an Jiaotong University. His research interests include wide bandgap power devices, package and integration, high density power conversion, wireless power transfer, and energy harvesting.

Prof. Wang is the recipient of Outstanding Young Scholar Award from China Power Supply Society (CPSS), China Electric Power Excellent Young Technological Talent Award from Chinese Society of Electrical Engineering. He is currently an Associate Editor for IEEE TRANSACTIONS ON POWER ELECTRONICS and IEEE JOURNAL OF EMERGING AND SELECTED TOPICS IN POWER ELECTRONICS. He is the Co-Chair of System Integration and Application in International Technology Roadmap for Wide Band-Gap Power Semiconductor, and the Chair of CPSS and IEEE PELS Joint Chapter in Xi'an, China.

Zaojun Ma (Student Member, IEEE) was born in Gansu Province, China, in 1993. He received the B.S. and M.S. degrees in electrical engineering from the Harbin Institute of Technology, Harbin, China, in 2016 and 2018, respectively. He is currently working toward the Ph.D. degree in electrical engineering with the Xi'an Jiaotong University, Xi'an, China.

His research interests include the packaging and application of wide bandgap devices and pulsed power technology.

Zhewei Zhang was born in Shaanxi Province, China, in 1998. He received the B.S. degree in electrical engineering from the Xi'an Jiaotong University, Xi'an, China, in 2020. He is currently working toward the Ph.D. degree in electronic and electrical engineering with the Xi'an Jiaotong University, Xi'an, China.

His research interests include the packaging and integration of wide bandgap power semiconductor devices.

Yan Wang was born in Jiangxi Province, China, in 2000. He received the B.S. degree in electrical engineering and automation from the Xi'an Jiaotong University, Xi'an, China, in 2021. He is currently working toward the master's degree in electrical engineering with the Xi'an Jiaotong University.

His research interests include the packaging and integration of wide bandgap power semiconductors and high-frequency power conversion technologies.

Kangping Wang (Senior Member, IEEE) received the B.S. and Ph.D. degrees in electrical engineering from the Xi'an Jiaotong University, Xi'an, China, in 2012 and 2018, respectively.

From August 2016 to August 2017, he was with the Department of ePOWER, Electrical and Computer Engineering, Queen's University, Kingston, ON, Canada, as a Visiting Scholar. Since 2018, he has been an Associate Professor with the School of Electrical Engineering, Xi'an Jiaotong University, Xi'an, China. His research interests include high-frequency power conversion technology, and application and integration technology of wide bandgap devices.

Dr. Wang was a recipient of the Best Paper Award of the International Conference on Power Electronics—ECCE Asia in 2019.

Xu Yang (Senior Member, IEEE) received the B.S. and Ph.D. degrees in electrical engineering from the Xi'an Jiaotong University, Xi'an, China, in 1994 and 1999, respectively.

Since 1999, he has been a member of the Faculty of School of Electrical Engineering, Xi'an Jiaotong University, where he is currently a Professor. From November 2004 to November 2005, he was with the Center of Power Electronics Systems, Virginia Polytechnic Institute and State University, Blacksburg, VA, USA, as a Visiting Scholar. He then came back to the Xi'an Jiaotong University, and engaged in the teaching and researches in power electronics and industrial automation area. His research interests include soft switching topologies, PWM control techniques, electromagnetic compatibility, power electronic integration, and packaging technologies.